Anomalous dynamics in symmetric triangular irrational billiards

Katerina Zahradova[a], Julia Slipantschuk[b], Oscar F. Bandtlow[a], Wolfram Just[a,1]

[a] *School of Mathematical Sciences, Queen Mary University of London, London, UK*
[b] *Department of Mathematics, University of Warwick, Coventry, UK*

Abstract

We identify a symmetry induced mechanism which dominates the long time behaviour in symmetric triangular billiards. We rigorously prove the existence of invariant sets in symmetric irrational billiards on which the dynamics is governed by an interval exchange transformation. Counterintuitively, this property of symmetric irrational billiards is analogous to the case of general rational billiards, and it highlights the non-trivial impact of symmetries in non-hyperbolic dynamical systems. Our findings provide an explanation for the logarithmic subdiffusive relaxation processes observed in certain triangular billiards. In addition we are able to settle a long standing conjecture about the existence of non-periodic and not everywhere dense trajectories in triangular billiards.

Keywords: Polygonal billiard, Recurrence, Induced map

2010 MSC: 37C83, 37C79

1. Introduction

The planar ballistic motion of a particle in a bounded region with elastic collision on the boundary, known as two-dimensional billiards, are among the simplest systems to illustrate the beauty and complexity of Hamiltonian dynamics. These paradigmatic models are the testing ground for exploring dynamical properties of physical systems by numerical and rigorous methods [1, 2], including quantum mechanical aspects [3, 4, 5]. Unlike billiards with curved boundaries, the seemingly simpler case of billiards with straight boundaries, known as polygonal billiards, add an additional challenge to the problem as there is no obvious mechanism to generate dynamical complexity. Here we consider the simplest instance of polygonal billiards, namely the ballistic motion of a point particle in a triangular domain. The simplest integrable cases, say billiards in an equilateral or symmetric right angled triangle, are among textbook examples of Hamiltonian systems, which can be reduced to the flow on a torus by the Zemlyakov-Katok construction [6]. However, these few examples are somewhat misleading as triangular billiards offer a plethora of rich dynamical behaviour.

Email addresses: k.zahradova@qmul.ac.uk (Katerina Zahradova), julia.slipantschuk@warwick.ac.uk (Julia Slipantschuk), o.bandtlow@qmul.ac.uk (Oscar F. Bandtlow), wolfram.just@uni-rostock.de (Wolfram Just)

[1] Present address: Institute of Mathematics, University of Rostock, Rostock, Germany

An important class of polygonal billiards which has attracted considerable interest from a rigorous perspective are those where the angles between sides are rational multiples of π. In this case each orbit only has a finite number of bouncing angles and this conservation law makes it possible to employ a machinery that allows for rigorous study of the underlying complex dynamical behaviour [7]. Unlike the previously mentioned integrable cases the dynamics can now be reduced to the flow on a complicated surface with singularities, and the dynamical features can be captured by suitable one-dimensional maps, known as interval exchange transformations [8]. This machinery is at the heart of rigorous studies of billiard dynamics. While the uniform distribution in rational billiards is not ergodic one is able to show, using techniques such as Rauzy induction [9], that the one-dimensional Lebesgue measure on the invariant set is ergodic. However, the seminal result of [10] proves that correlations do not decay, i.e., that the related interval exchange transformation is never mixing.

For triangular billiards with angles irrational multiples of π little to nothing is known from a rigorous perspective. A notable exception is the seminal result [11] which establishes ergodicity of the uniform distribution in phase space, i.e., ergodicity of the microcanonical distribution, for a topologically large class of billiards. Whether that statement actually applies to a large class of billiards, say for Lebesgue almost all angles, is to the best of our knowledge still unknown. Moreover, there are only few explicit cases of billiards where ergodicity of the two-dimensional Lebesgue measure has been established [12]. To the the best of our knowledge, nothing is known about correlation decay from a rigorous perspective, though this question has been revisited in the last two decades [13]. So far, results are not fully conclusive [13, 14, 15, 16, 17] claiming evidence for decay of correlations or lack of decay. In some cases the difference is attributed to certain number-theoretic properties of the angles involved. But even the ergodicity of the uniform distribution is not obvious, apart from a few cases where rigorous results are available [12]. It seems that certain irrational billiards exhibit very long transients, with statements to that extent in the literature [18, 15], but no convincing studies seem to be available.

Here we will address this issue and provide a potential solution for this conundrum, namely, that the anomalous behaviour in triangular billiards can be attributed to the symmetry of the triangle [19]. While we will also present numerical evidence, the main part of our exposition is a rigorous analysis where we prove the existence of symmetry-induced invariant sets which are at the heart of the observed anomalous behaviour. In section 2 we will introduce the notation and provide a numerical example to show the impact of the slow relaxation process in symmetric triangular billiards. The main cause, namely recurrence properties in triangular billiards will be reviewed in section 3, where we show that this feature is intimately linked with the symmetry of the system. The main tool, the one-dimensional induced map, is introduced in section 4. This approach enables us to identify complex invariant sets in the phase space of symmetric triangular billiards by analytic means. As an aside we will also settle a long standing conjecture [20, 21] about non-periodic, not everywhere dense orbits in the configuration space of triangular billiards. Finally, in section 5

we will demonstrate the existence of logarithmic subdiffusion of the momentum in symmetric billiards. The conclusion will outline the impact of our rigorous studies for the numerical findings and provide a roadmap for further investigations of polygonal billiards.

2. Billiard map

In order to fix the notation consider the ballistic motion of a point particle in a triangular domain with elastic collisions at the boundary. The geometry is shown in figure 1.

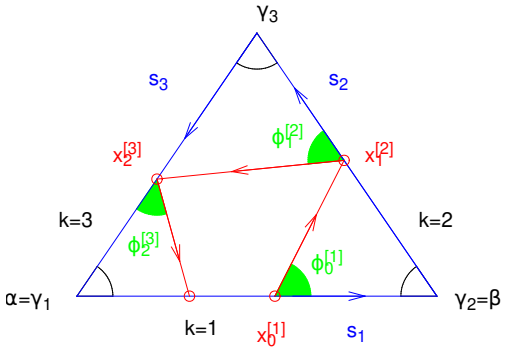

Figure 1: Diagrammatic view of a triangular billiard with internal angles γ_k and sides of lengths s_k. An orbit of finite length with initial condition $(k_0 = 1, x_0^{[1]}, \phi_0^{[1]})$ is indicated where the sequence of bouncing sides (k_0, k_1, k_2) is given by $(1, 2, 3)$. The bouncing angle is denoted by $\phi_t^{[k_t]}$ and the location of bounces is given by $x_t^{[k_t]}$.

We label the three sides of the triangle by a cyclic index $k = 1, 2, 3$, and we assume that the sides are oriented counter-clockwise. The length of side k is denoted by s_k, while γ_k and γ_{k+1} denote the left or right angle at side k, respectively. We shall consider cases where these angles are irrational multiples of π. We call side $k = 1$ the base, we choose units of length such that $s_1 = 1$, and we abbreviate the angles on the base by $\alpha = \gamma_1$ and $\beta = \gamma_2$. We call a triangle symmetric if $\alpha = \beta$. We denote by $x^{[k]} \in [0, s_k]$ the position at which an orbit bounces on side k and by $\phi^{[k]} \in [0, \pi]$ the angle between the outgoing ray and the oriented side. The conjugate canonical variable $p^{[k]} = \cos(\phi^{[k]}) \in [-1, 1]$ can be used to write down the dynamics as a Hamiltonian system. We call a move counter-clockwise (ccw) if the bounce on side k is followed by a bounce on side $k + 1$, while a move is called clockwise (cw) if a bounce on side k is followed by a bounce with side $k - 1$. All moves indicated in figure 1 are counter-clockwise moves.

We call an orbit singular if it hits some of the corners in finite time. For the infinite time dynamics we exclude singular orbits and restrict the discussion to regular orbits. Subsequent bounces are related by the billiard map

$$\phi_{t+1}^{[k_{t+1}]} = \begin{cases} \pi - \phi_t^{[k_t]} - \gamma_{k_{t+1}} & \text{if} \quad k_{t+1} = k_t + 1 \text{ (ccw)} \\ \pi - \phi_t^{[k_t]} + \gamma_{k_t} & \text{if} \quad k_{t+1} = k_t - 1 \text{ (cw)} \end{cases}$$

$$x_{t+1}^{[k_{t+1}]} = \begin{cases} (s_{k_t} - x_t^{[k_t]}) \sin(\phi_t^{[k_t]}) / \sin(\phi_{t+1}^{[k_{t+1}]}) & \text{if (ccw)} \\ s_{k_{t+1}} - x_t^{[k_t]} \sin(\phi_t^{[k_t]}) / \sin(\phi_{t+1}^{[k_{t+1}]}) & \text{if (cw)} \end{cases} \quad (1)$$

There are different ways to visualise orbits in phase space. Here we decide to record only bounces on the base, i.e., formally we induce the dynamics on the base $k = 1$, as the time between subsequent bounces on the base is finite and bounded. If we use the abbreviation $x = x^{[1]}$ and $p = p^{[1]}$ the phase space is the rectangle $\{(x, p) : 0 \leq x \leq 1, -1 < p < 1\}$. The seminal result [11] suggests that for triangles where the angles are irrational multiples of π, known as irrational billiards, a typical orbit spreads out uniformly in phase space, i.e., the two-dimensional Lebesgue measure is ergodic. Figure 2 shows the initial part of such a typical orbit in a symmetric and a slightly perturbed symmetric triangle, where one observes a striking difference. While in the asymmetric case the orbit points spread out fast and seemingly cover the phase space uniformly a strange localisation phenomenon is observed for symmetric triangles where angle or momentum take on very few values only and the spreading is very slow, or non-existent. This type of dynamical signature superficially resembles that seen in rational billiards, an observation that has been reported in the literature previously [15, 17], but the potential connection with symmetries has never been highlighted. In this paper the mechanism underpinning this slow relaxation phenomenon is at the heart of our interest, and we will provide both a rigorous analysis and numerical calculations.

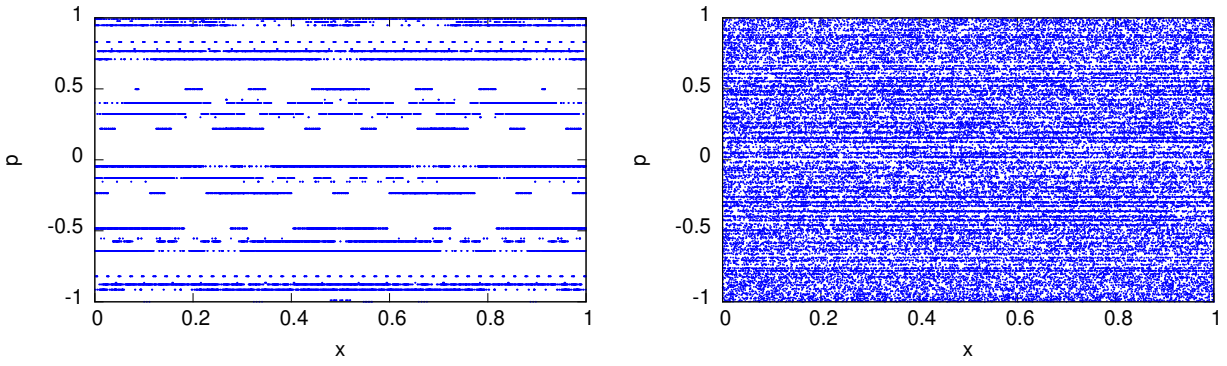

Figure 2: Orbit of length $T = 10^6$ with initial condition $x_0 = 1/\sqrt{2}$ and $p_0 = \cos(0.7)$ in a triangular billiard, shown in the phase space induced on the base. Left: symmetric billiard with $\alpha = \beta = \pi(\sqrt{5} - 1)/4$, right: weakly asymmetric billiard with $\beta = \alpha - \varepsilon$ where $\alpha = \pi(\sqrt{5} - 1)/4$ and $\varepsilon = 10^{-5}$.

3. Recurrence

As shown in figure 2, the striking difference between the dynamics in symmetric and asymmetric triangles is most vividly illustrated by considering the momentum or the bouncing angle. Consequently, we shall now take a closer look at the momentum dynamics. Eq.(1) tells us that the angle can be written as

$$\phi_t^{[k_t]} = n_t^{\pi}\pi + n_t^{\alpha}\alpha + n_t^{\beta}\beta + n_t^{\phi}\phi_0 \quad (2)$$

where the integers n_t^π, n_t^α, n_t^β, and n_t^ϕ obey the initial condition $n_0^\pi = n_0^\alpha = n_0^\beta = 0$, $n_0^\phi = 1$. The updating rules for these integers can be easily derived from eq.(1). A closer look at these rules reveals that the moduli of the integers change by at most one per time step. The rule for the last integer is particularly simple, namely $n_t^\phi = (-1)^t$. Closed-form expressions for the remaining ones, however, cannot be derived. Nevertheless, eq.(2) and the updating rules for the integers allow us to capture the momentum dynamics without any numerical rounding errors. Computing the momentum is straightforward and gives

$$p_t^{[k_t]} = (-1)^{n_t^\pi} \cos\left(m_t(\alpha+\beta)/2 + d_t(\alpha-\beta)/2 + \phi_0\right) \tag{3}$$

where

$$m_t = (-1)^t \left(n_t^\alpha + n_t^\beta\right), \quad d_t = (-1)^t \left(n_t^\alpha - n_t^\beta\right) . \tag{4}$$

The indices defined in eq.(4) change by at most two per time step. Hence they suitably parameterise the momentum $p_t^{[k_t]}$ relative to the initial momentum. In particular, for symmetric triangles the momentum is essentially given by the index m_t only. The idea to capture the momentum dynamics by integer quantities has been proposed previously in [17].

In order to understand the underlying features visible in figure 2 we consider an orbit starting on the base $k_0 = 1$ at $x_0 = x_0^{[1]}$ with momentum $p_0 = p_0^{[1]}$ and compute the shortest positive time $t = T_{rec}$ such that the momentum returns to its initial value on the base $p_t^{[k_t=1]} = p_0$. In general, employing this kind of induction procedure for a dynamical system with continuous phase space is meaningless. However, the present case is different as the angles and the momentum take on discrete values only, see eq.(3) or (4). Moreover, the recurrence condition can be easily phrased in terms of the integer indices, eq.(4). Figure 3 contains results for the recurrence times when we scan the phase space of initial conditions.

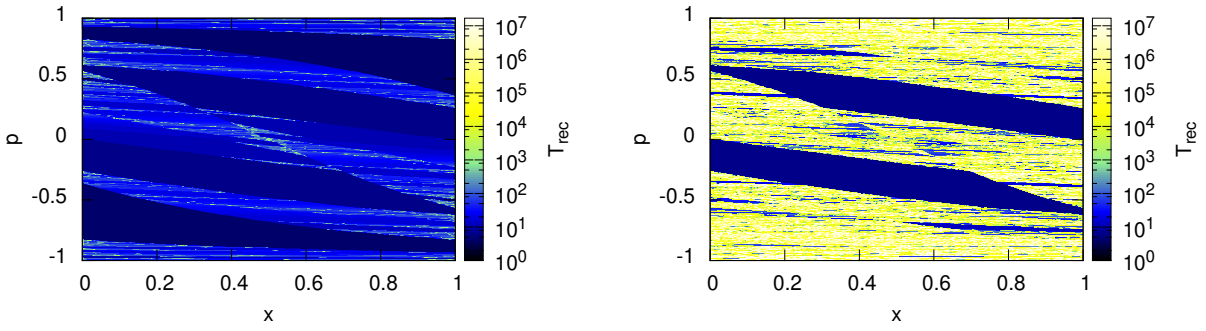

Figure 3: Recurrence times $t = T_{rec}$ for the induction $p_t^{[k_t=1]} = p_0$ computed for a regular grid of 500×500 initial conditions in phase space. Left: symmetric billiard with $\alpha = \beta = \pi(\sqrt{5}-1)/4$, right: weakly asymmetric billiard with $\beta = \alpha - \varepsilon$ where $\alpha = \pi(\sqrt{5}-1)/4$ and $\varepsilon = 10^{-5}$ (cf. figure 2).

When comparing symmetric with asymmetric triangles, the corresponding recurrence plots differ significantly. It seems that in the symmetric case, for a large set of initial conditions, the recurrence time stays finite, while in the asymmetric case recurrence times may be unbounded for a large set of initial conditions.

From now on we will focus exclusively on the symmetric case $\alpha = \beta$. The mechanism for the prevalence of recurrent orbits in symmetric cases can be pinned down to the existence of a very large number of recurrent orbits induced by the symmetry of the triangle. For that purpose consider first an orbit starting on the base at $x = 1/2$ which after a finite number of bounces ends on the base again. The symmetric image of this orbit, i.e., reflecting the orbit at the symmetry axis of the triangle gives again an orbit starting at $x = 1/2$ with opposite momentum. If we reverse the momenta of this part and glue both parts together we obtain by construction a symmetric recurrent orbit with even recurrence time T_{rec}, $p^{[1]}_{T_{rec}} = p_0$, starting on the base at $x^{[1]}_0$ and ending on the base at $x^{[1]}_{T_{rec}} = 1 - x^{[1]}_0$, see figure 4. In fact all symmetric recurrent orbits starting and ending on the base are of this type as, by symmetry, the midpoint is on the base at $x = 1/2$. Thus symmetric triangles admit a countable infinite number of continuous families of symmetric recurrent orbits of even recurrence time.

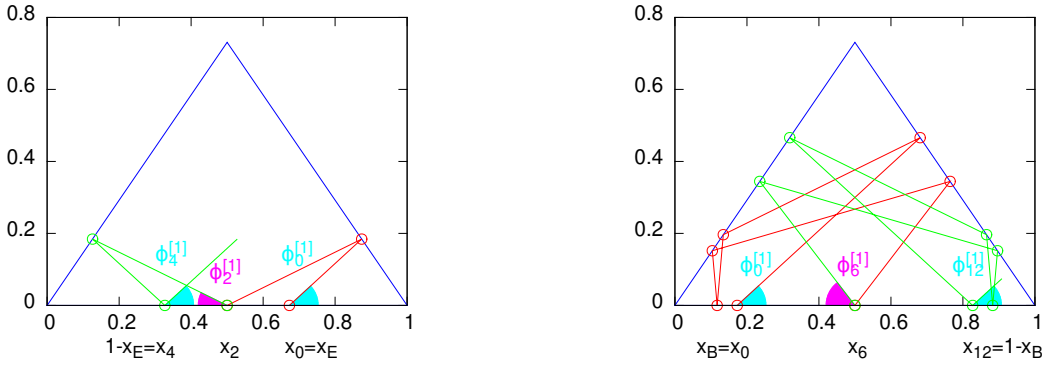

Figure 4: Symmetric recurrent orbits of even length T_{rec} in a symmetric triangle with initial condition x_0 and $p_0 = \cos(\phi^{[1]}_0)$ on the base. The endpoint $x^{[k_{T_{rec}}=1]}_{T_{rec}} = 1 - x_0$ and $p^{[k_{T_{rec}}=1]}_{T_{rec}} = p_0$ is on the base as well. The two symmetric halves of the orbit are coloured in red and green respectively. Left: orbit with recurrence time $T_{rec} = 4$ and initial position $x_0 = x_E$, right: orbit with recurrence time $T_{rec} = 12$ and initial position $x_0 = x_B$ (cf. figure 5).

Let us exclude the singular case where the endpoints of the symmetric orbit are at the corners of the triangle, giving rise to what is known as a heteroclinic orbit. Then the position of bounces of the symmetric recurrent orbit have finite distance from the singularities, i.e., finite distance from the corners of the triangle. Consider a recurrent orbit of even length T_{rec}. A sufficiently small change of the initial conditions x_0 and p_0 will give rise to a continuous change of orbit points, see eq.(1), as long as none of those points hits one of the corners. Hence the sequence of bouncing sides, $(k_t)_{0\le t\le T_{rec}}$, as well as the integers in eq.(2) remain unchanged. Thus, under a small change of initial conditions , the orbit still satisfies $\phi^{[k_{T_{rec}}]}_{T_{rec}} = (-1)^{T_{rec}}\phi^{[1]}_0 = \phi^{[1]}_0$, which means that the perturbed orbit is still recurrent. Thus the set of regular recurrent orbits of even length is an open set. Furthermore each of the symmetric recurrent orbits comes with an open neighbourhood of recurrent orbits of the same bouncing side sequence $(k_t)_{0\le t\le T_{rec}}$. In that sense the symmetric recurrent orbits provide a skeleton for the recurrence plot of symmetric triangles shown in figure 3. We presume that the set of even recurrent orbits is a dense set of the recurrence plot,

perhaps even of full Lebesgue measure, but so far we have no formal proof of this conjecture.

Furthermore, symmetric triangles also admit recurrent orbits of odd length, but they are residual in the following sense A symmetric orbit of odd length does not have a central node, but a central link. By symmetry this link is horizontal. Thus, starting from a horizontal link a symmetric recurrent orbit of odd length T_{rec} is obtained by backward and forward iteration by the same number of steps. The same continuity argument used above shows that changing the initial position $x_0 = x_0^{[1]}$ slightly and keeping the initial momentum fixed gives again a recurrent orbit of odd length. However, if we change the initial angle by a small amount $\Delta\phi_0$ then eq.(2) tells us that the final angle changes by $\Delta\phi^{[1]}_{T_{rec}} = (-1)^{T_{rec}}\Delta\phi_0 = -\Delta\phi_0$ and the recurrence condition is violated. Hence odd recurrent orbits are isolated objects and are almost impossible to detect in direct numerical scans. In fact, the recurrence plot shown in figure 3 only contains recurrent orbits of even length.

4. Induced map

For symmetric triangles, $\alpha = \beta$, it is tempting to consider horizontal slices in the recurrence plot, figure 3, and to investigate whether those yield a well-defined one-dimensional dynamical system. In fact such induced maps with inducing on the real-valued initial momentum, $p_t^{[k_t=1]} = p_0$, can be introduced rigorously for symmetric triangles. To illustrate first the main mechanism we consider a symmetric triangle with $\alpha = \pi/4(\sqrt{5}-1)$ and the special value $p_0 = p_{R4R12} = 0.737113\ldots$, a choice we are going to justify later in the course of this section, see eq.(9). This particular induction results in the well-defined induced map shown in figure 5. In the following we shall discuss in detail the mechanisms leading to the one-dimensional map governing the motion of the two-dimensional billiard dynamics.

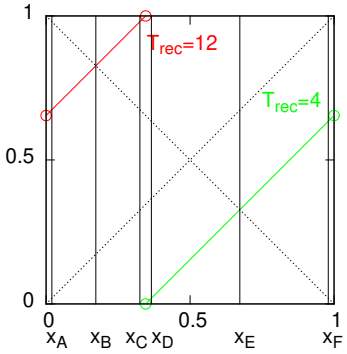

Figure 5: Induced map of a symmetric triangle with $\alpha = \beta = \pi(\sqrt{5}-1)/4$ and induction condition $p^{[k_{T_{rec}}=1]}_{T_{rec}} = p_0 = p_{R4R12}$. The value of the recurrence time is indicated as well. The points x_{A-F} are the mid- and endpoints of the intervals over which the induced map is defined, cf. figures 4 and 6.

Each point x in the interval $[0,1]$ over which the induced map is defined represents an initial condition $(x, p_0 = p_{R4R12})$ on the base $k_0 = 1$, which gives rise to a finite orbit with recurrence time T_{rec}. In the present

case the two branches of the induced map correspond to 4-recurrent and 12-recurrent orbits respectively. If we consider the value x_E, see figure 5, which is mapped to $1-x_E$, then the corresponding 4-recurrent orbit is the symmetric 4-recurrent orbit shown in figure 4. As previously discussed, changing the initial condition x_E by a small amount Δx_0, such that orbit points of the recurrent orbit do not hit any of the corners, gives rise to a continuous change of the endpoint $x_{T_{rec}}^{[1]}$ which determines the branch of the induced map. This change can be easily evaluated from eq.(1) as the corresponding variational equation stays linear and hence can be solved easily. Changing the initial location by Δx_0 and keeping the initial momentum fixed the orbit at time t, $x_t^{[k_t]}$, changes by

$$\Delta x_t^{[k_t]} = (-1)^t \Delta x_0 \sin(\phi_0^{[1]}) / \sin(\phi_t^{[k_t]}) \,. \tag{5}$$

Since, by recurrence, $\phi_{T_{rec}}^{[k_{T_{rec}}]} = \phi_0^{[1]}$ we conclude that $\Delta x_{T_{rec}}^{[k_{T_{rec}}]} = \Delta x_0$. This gives rise to a linear branch emanating from $(x_E, 1-x_E)$ with slope one, as shown in figure 5. In addition the symmetry of the triangle gives rise to conjugate pairs of orbits. If we reflect a recurrent orbit at the symmetry axis of the triangle and revert the momenta, we again obtain a recurrent orbit of the same length and with the same momentum $p_0 = p_{R4R12}$. The induced map maps $x_E+\Delta x_0$ to $1-x_E+\Delta x_0$ so that the recurrent orbit starting at $x_E+\Delta x_0$ ends at $1-x_E+\Delta x_0$. If we apply the conjugacy mentioned above we obtain a recurrent orbit starting at $1-(1-x_E+\Delta x_0) = x_E - \Delta x_0$. Hence the two points $x_E \pm \Delta x_0$ give rise to a conjugate pair of recurrent orbits which are related by reflection at the symmetry axis and reversing the momenta. Our considerations so far have been general, they apply to any induced map. Thus a symmetric recurrent orbit gives rise to a branch of the induced map with slope one which is symmetric around the antidiagonal. The resulting one-dimensional map is a so-called symmetric interval exchange transformation [22], if the construction can be performed on the entire domain $[0,1]$. For the current choice of p_0 we have just obtained two branches, see figure 5, which results in the simple case of a rotation.

Let us now focus on the discussion of the endpoints x_D and x_F of the 4-recurrent interval, see figure 5, over which a branch of the rotation is defined. As mentioned above, on the one hand these two points give rise to conjugate orbits and on the other hand these orbits hit one of the corners. To discuss this singular case we assume an infinitesimal distance from the singularity, i.e., x_D and x_F are within the open interval over which the branch of the induced map is defined. Figure 6 shows the 4-recurrent singular orbit starting at $x_0^{[1]} = x_D$ (and the conjugate image of the orbit starting at x_F). After two iterations the orbit hits the singularity, and then becomes recurrent after four steps. Hitting the singularity gives rise to the discontinuity of the induced map and eq.(5) allows us to compute the interval $[x_D, x_F]$ (that means the maximal possible value for Δx_0) easily. We only need to check the four constraints $0 \le x_t^{[k_t]} + \Delta x_t^{k_t} \le s_{k_t}$ for $1 \le t \le T_{rec}$. Again, the fact that singular orbits determine the discontinuities of the induced map and the computation of the intervals over which the resulting interval exchange transformation is defined is a general feature which is not specific to the special case discussed here.

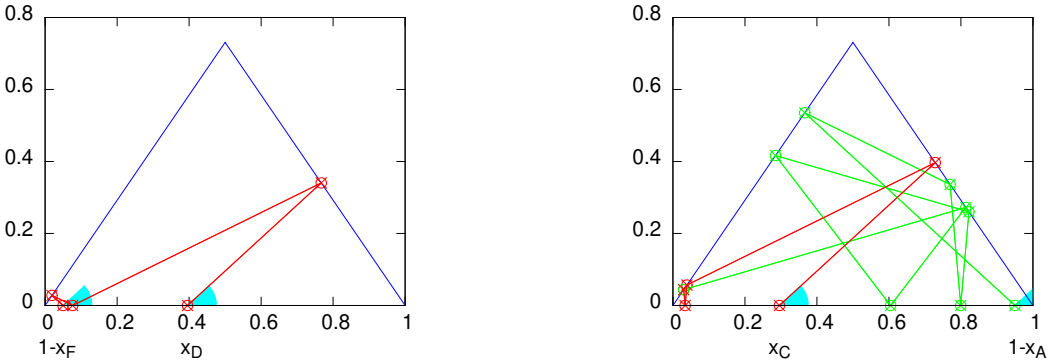

Figure 6: Recurrent orbits for a symmetric triangle with $\alpha = \beta = \pi(\sqrt{5}-1)/4$ for the induced map shown in figure 5 with $p_0 = p_{R4R12}$. Left: 4-recurrent orbit (circles) starting on the base at x_D and ending at $1 - x_F$ (see figure 5). Recall that for reasons of visibility the initial condition has been slightly moved away from the discontinuity of the one-dimensional induced map, and that the three final points of the orbit coincide in the limit of x_D approaching the discontinuity. Crosses are the conjugate (i.e. reflected and reversed) of the recurrent orbit starting at x_F and ending at $1 - x_D$. Right: 12-recurrent orbit (circles) starting at x_C and ending at $1 - x_A$ (see figure 5). Again, for reasons of visibility initial conditions have been slightly moved away from the discontinuity. Since x_C and x_D are infinitesimally close initial conditions in phase space, the initial part of the orbit (coloured in red, $0 \le t \le 4$) coincides with the orbit shown in the left figure. The final part of the orbit (coloured in green, $4 \le t \le 12$) yields the heteroclinic part connecting two singularities (in the limit of x_C approaching the discontinuity). Crosses are the conjugate (i.e. reflected and reversed) of the recurrent orbit starting at x_A and ending at $1 - x_C$.

If we cross the discontinuity at x_D and consider the coordinate x_C on the "other side" of the discontinuity we obtain an orbit which initially coincides with the orbit emanating from x_D, as in phase space the two initial conditions are infinitesimally close. However, the orbit emanating from x_C hits the corner from the opposite side of the triangle, it then deviates from the orbit emanating from x_D, and it does not become recurrent after 4 iterations, see figure 6. Instead we have to wait for another 8 iterations to meet the recurrence condition, so that this new branch of the induced map corresponds to a recurrence time $T_{rec} = 12$. Thus, the orbit hitting the singularity is the cause for the discontinuity in the induced map. The midpoint of the 12-recurrent branch at x_B gives rise to the symmetric 12-recurrent orbit shown in figure 4, and the left interval endpoint at x_A corresponds to the conjugate orbit at x_C, see figure 6. These three values, x_A, x_B and x_C, can be computed as outlined above and this calculation shows that the two branches of the rotation cover the full domain $[0, 1]$. Hence our induced map is well defined and covers the whole billiard dynamics with initial momentum p_0 and initial condition on the base. As already outlined above the orbit at the discontinuity x_C and its conjugate at x_A are singular orbits. In addition, since the induced map maps x_C to one, the endpoint of this orbit is the right corner of the triangle. Hence this orbit connects two singularities (see figure 6) which are met at $x_4^{[2]}$ and $x_{12}^{[1]}$ when considering the orbit emanating from x_C, or which are met at $x_0^{[1]} = x_A$ and $x_8^{[2]}$ when considering the conjugate orbit starting at x_A (see figure 6, recall that in the limit when the initial condition approaches the discontinuity there are three orbit points converging towards the singularity). Such a heteroclinic orbit is the key element which determines the properties of the induced map and the particular value of the momentum $p_0 = p_{R4R12}$.

The heteroclinic connection with $x_0^{[1]} = 0$ and $x_8^{[2]} = 1$ (see figures 6 and 7) has the sequence of bouncing

sides $(k_t)_{0\le t\le 8} = (1,2,3,1,3,2,1,3,2)$. Using the iteration of eq.(1) we obtain for the bouncing angles

$$\begin{aligned}
&\phi_1^{[2]} = \pi - \phi_0^{[1]} - \alpha, && \phi_2^{[3]} = -\pi + \phi_0^{[1]} + 3\alpha, && \phi_3^{[1]} = 2\pi - \phi_0^{[1]} - 4\alpha \\
&\phi_4^{[3]} = -\pi + \phi_0^{[1]} + 5\alpha, && \phi_5^{[2]} = 3\pi - \phi_0^{[1]} - 7\alpha, && \phi_6^{[1]} = -2\pi + \phi_0^{[1]} + 8\alpha \\
&\phi_7^{[3]} = \phi_5^{[2]}, && \phi_8^{[2]} = \phi_4^{[3]}\,.
\end{aligned} \tag{6}$$

For the spatial coordinate eq.(1) gives

$$\begin{aligned}
&x_0^{[1]} = 0, && x_1^{[2]} = (s_1 - x_0^{[1]})\tfrac{\sin(\phi_0^{[1]})}{\sin(\phi_1^{[2]})}, && x_2^{[3]} = (s_2 - x_1^{[2]})\tfrac{\sin(\phi_1^{[2]})}{\sin(\phi_2^{[3]})} \\
&x_3^{[1]} = (s_3 - x_2^{[3]})\tfrac{\sin(\phi_2^{[3]})}{\sin(\phi_3^{[1]})}, && x_4^{[3]} = s_3 - x_3^{[1]}\tfrac{\sin(\phi_3^{[1]})}{\sin(\phi_4^{[3]})}, && x_5^{[2]} = s_2 - x_4^{[3]}\tfrac{\sin(\phi_4^{[3]})}{\sin(\phi_5^{[2]})} \\
&x_6^{[1]} = s_1 - x_5^{[2]}\tfrac{\sin(\phi_5^{[2]})}{\sin(\phi_6^{[1]})}, && x_7^{[3]} = s_3 - x_6^{[1]}\tfrac{\sin(\phi_6^{[1]})}{\sin(\phi_7^{[3]})}, && x_8^{[2]} = s_2 - x_7^{[3]}\tfrac{\sin(\phi_7^{[3]})}{\sin(\phi_8^{[2]})} = 0\,.
\end{aligned} \tag{7}$$

If we eliminate the spatial coordinates by iteration and use $1 = s_1 = 2\cos(\alpha)s_2 = 2\cos(\alpha)s_3$ eq.(7) simplifies to

$$\begin{aligned}
0 \;=\; & -\sin(\phi_8^{[2]}) + \sin(\phi_7^{[3]}) - 2\cos(\alpha)\sin(\phi_6^{[1]}) + \sin(\phi_5^{[2]}) - \sin(\phi_4^{[3]}) + \sin(\phi_2^{[3]}) \\
& - \sin(\phi_1^{[2]}) + 2\cos(\alpha)\sin(\phi_0^{[1]})\,.
\end{aligned} \tag{8}$$

In fact, the structure of this condition is solely determined by the symbolic bouncing side sequence of the heteroclinic orbit. Finally inserting the bouncing angles from eq.(6) we arrive at the expression which determines $\phi_0^{[1]}$ and $p_0 = \cos(\phi_0^{[1]})$

$$0 = 2\sin(\phi_0^{[1]} + 6\alpha) - \sin(\phi_0^{[1]} + 8\alpha) - \sin(\phi_0^{[1]} + 2\alpha) + \sin(\phi_0^{[1]})\,. \tag{9}$$

This equation has a unique solution for $\phi_0^{[1]} \in [0,\pi]$ which then gives the value of $p_0 = p_{R4R12}$. This value can even be expressed in closed analytic form.

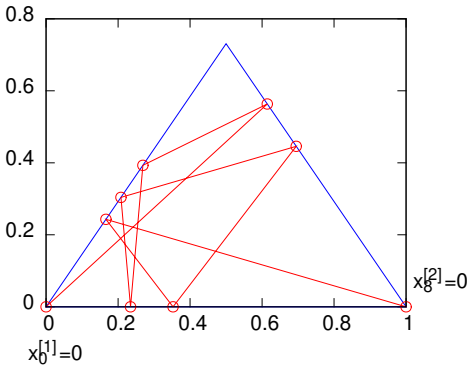

Figure 7: Heteroclinic orbit for a symmetric triangle with $\alpha = \beta = \pi(\sqrt{5}-1)/4$ and induction on $p_0 = p_{R4R12}$, starting at $x_0^{[1]} = 0$ and ending at $x_8^{[2]} = 0$ (see figure 6, green part, for the conjugate orbit).

All that remains now is computing the position of the discontinuity of the induced map at x_D (or equivalently at x_C). The orbit emanating form x_D (see figure 6 left) gives $x_0^{[1]} = x_D$, $x_2^{[1]} = 0$ with sequence

of bouncing sides $(k_t)_{0\leq t\leq 2} = (1, 2, 1)$. As before this sequence and eq.(1) results in the bouncing angles

$$\phi_1^{[2]} = \pi - \phi_0^{[1]} - \alpha, \quad \phi_2^{[1]} = \phi_0^{[1]} + 2\alpha \tag{10}$$

while for the spatial coordinates we obtain

$$x_1^{[2]} = (s_1 - x_0^{[1]})\frac{\sin(\phi_0^{[1]})}{\sin(\phi_1^{[2]})},\ x_2^{[1]} = s_1 - x_1^{[2]}\frac{\sin(\phi_1^{[2]})}{\sin(\phi_2^{[1]})} = 0\,. \tag{11}$$

Solving for $x_0^{[1]} = x_D$ finally yields

$$x_D = 1 - \sin(\phi_0^{[1]} + 2\alpha)/\sin(\phi_0^{[1]}) \tag{12}$$

which also determines the rotation number of the induced map shown in figure 5.

For our analysis we have not resorted to any particular feature of the value α. Hence the induced map exists for a large range of triangles as long as the shape of the triangle supports the particular 4- and 12-recurrent orbits shown in figure 6. In particular, number theoretic properties of α are of no special relevance for our considerations. For the special value $\alpha = \pi(\sqrt{5}-1)/4$ evaluation of eqs.(9) and (12) together with an appeal to the Lindemann-Weierstrass theorem (see, e.g., [23]) proves that the induced map is an irrational rotation.

The results so far can be nicely summarised by constructing the unfolding of the billiard dynamics for orbits starting on the base with bouncing angle ϕ_0, $p_0 = \cos(\phi_0)$, see figure 8 . Depending on the starting position on the base, $x_A < x < x_C = x_D$ or $x_C = x_D < x < x_F$, the unfolding shows a 12- respectively 4-recurrence structure. The symmetry of the triangle ensures that the first half of this structure is the mirror image of the second half (see also figure 4) so that the recurrence condition on the base is automatically satisfied. In addition, singular orbits determine the domain and discontinuities of the induced map at x_A, $x_C = x_D$, and x_F (see also figure 6), while the heteroclinic orbit of length 8 determines the momentum value p_0 (see also figure 7). If one glues the corresponding parts on the base one obtains a compact manifold and the dynamics is governed by the rotation map, figure 5. The unfolding shows also that the rotation map can be constructed for a whole range of symmetric triangles and that one typically obtains an irrational ergodic rotation. We also note, that incidentally we have provided an answer to a question raised in [20] , namely whether every non-periodic orbit in a triangular billiard is everywhere dense in configuration space. While the solution proposed in [20] contained a major flaw, as pointed out in [21], our approach proves that there exist symmetric triangular billiards with orbits which are neither dense in configuration space nor periodic, see our previous considerations and figure 8. The unfolding clearly proves that orbits never cover the whole triangle as they miss a small region near the tip of the triangle, while aperiodicity is a consequence of the irrational rotation map. Details of an abstract proof will be published elsewhere.

The induced map is defined on the line $\{(x, p_0 = p_{R4R12}) : 0 \leq x \leq 1\}$ in the two-dimensional phase space of the symmetric triangular billiard. The one-dimensional induced map comes with a corresponding

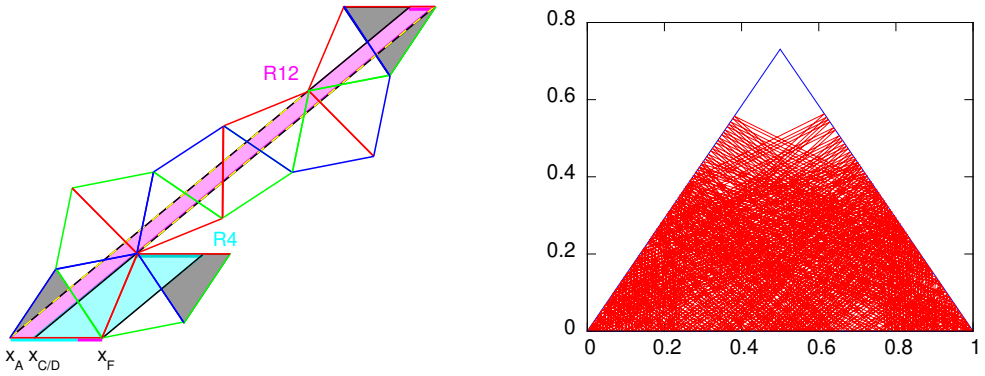

Figure 8: Left: Diagrammatic view of the unfolding of the billiard dynamics for a symmetric triangle with $\alpha = \pi(\sqrt{5}-1)/4$ and initial momentum $p_0 = p_{R4R12}$ on the base (cf. figure 5). The base of the triangle is shown in red and the two other sides in green and blue. The initial and final triangles are shaded. Singular orbits which determine the domain and the discontinuity of the induced map are shown in black, the heteroclinic orbit of length 8 which determines the momentum p_0 is shown in yellow-dashed. The 12- and 4-recurrent regions are indicated in magenta and cyan, respectively. The correspondingly coloured (magenta, cyan) horizontal parts on the base indicate how to identify the sides to obtain a compact surface. Right: Corresponding trajectory in configuration space for a symmetric billiard with $\alpha = \pi(\sqrt{5}-1)/4$. The trajectory has length $T = 500$ with initial condition $x_0 = 1/\sqrt{2}$ and $p_0 = p_{R4R12}$ on the base.

invariant set in this phase space. Using the billiard map we can lift the line on which the induced map has been defined to the whole phase space by iteration. Clearly this invariant set contains only four admissible angles $\{\phi_0^{[1]}, \phi_0^{[1]} + 2\alpha, 2\pi - \phi_0^{[1]} - 4\alpha, -2\pi + \phi_0^{[1]} + 8\alpha\}$ (see eqs.(6) and (10)) and the full set can be easily constructed from the orbits shown in figure 6 and the coordinates defined in eqs.(7) and (11), see figure 9. While inducing the dynamics by $p_t^{[k_t=1]} = p_0$ worked over the full range of x-values, one can also induce over subsets of x-values for the other angles. This results again, by construction, in well-defined induced maps, see figure 9. This trivial illustration shows that inducing offers a large range of options to construct well-defined interval exchange transformations and corresponding invariant sets for the billiard dynamics.

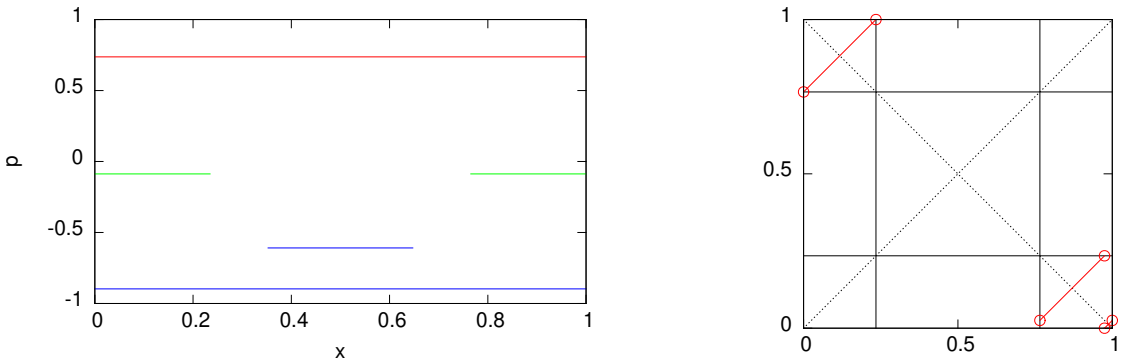

Figure 9: Left: Invariant set of a billiard in a symmetric triangle with $\alpha = \beta = \pi(\sqrt{5}-1)/4$, which results from lifting the line $p = p_{R4R12}$ (red) to the phase space. Inducing the billiard dynamics on this line results, by construction, in the induced map shown in figure 5. Right: Induced map obtained by inducing the billiard dynamics on the green subset.

As shown by our example the construction of well-defined induced maps requires a basic understanding of recurrent orbits, or more generally of the bouncing sequences in triangular and polygonal billiards.

From a general point of view, considerable progress has been made recently [24, 25, 26, 27], but the issue remains far from being settled, in particular for irrational triangles. However, the analytic principles used for constructing this simple example of a well-defined non-trivial one-dimensional induced map are easily extended to cover highly non-trivial cases. The choice $p_0 = 0.7113433\ldots$ and inducing the momentum over the full range of x-values results in a well defined interval exchange transformation with recurrence times as large as $T_{rec} = 258784$, see figure 10. The heteroclinic orbit of length 212736 which appears at the interval endpoints of the interval with the highest recurrence time $T_{rec} = 258784$ determines the momentum p_0 used in the induction. Furthermore, in configuration space none of the orbits gets close to the tip of the triangle, so that there is again, as before, an open neighbourhood of the tip of the triangle which is not met by any of the trajectories. Thus, we have another example for non-dense orbits in configuration space,

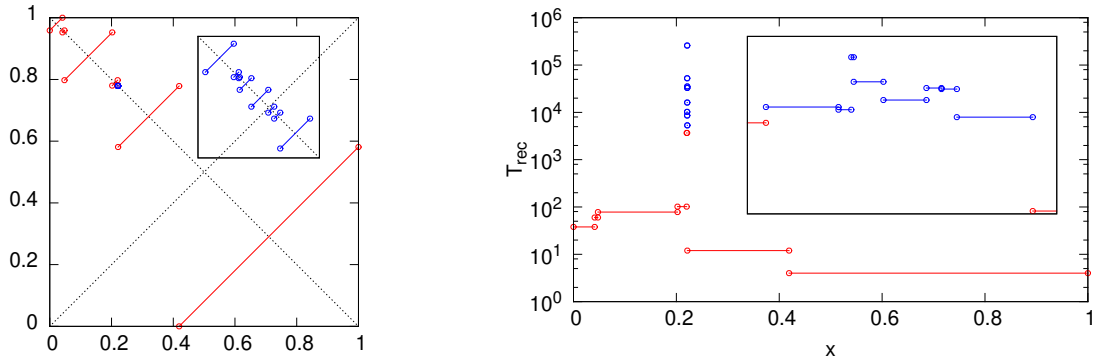

Figure 10: Left: Well-defined induced map for the dynamics in a symmetric triangle with $\alpha = \beta = \pi(\sqrt{5}-1)/4$. The induction condition on the momentum reads $p_t^{[k_t=1]} = p_0 = 0.7113433\ldots$. The inset shows the blue part on a finer scale. Right: corresponding recurrence times of the induced map. The inset shows the blue part on a finer scale.

The induced map, figure 10, is defined on the line $\{(x, p_0) : 0 \leq x \leq 1\}$ in phase space. As before, we can lift this line to an invariant set in phase space which contains all the points which occur while iterating the billiard map, see figure 11. Surprisingly, this invariant set of the billiard dynamics resembles, at a qualitative level, the structures visible in a finite time numerical simulation of the billiard dynamics, cf. figure 2.

5. Logarithmic subdiffusion

As pointed out previously, symmetric triangular billiards exhibit an anomalous relaxation process compared to general triangular billiards. Our analytic approach is able to provide a qualitative explanation for this phenomenon. Very slow relaxation in triangular irrational billiards have been reported over the course of the last decades [13, 15, 17] but the findings have not been fully conclusive. In almost all cases this behaviour has been attributed to some number theoretic properties of the angles of the triangle but no convincing evidence was provided. Only recently the role of symmetry has been emphasised [19], but no further analytic explanation has been provided so far. To begin with we first summarise numerical findings

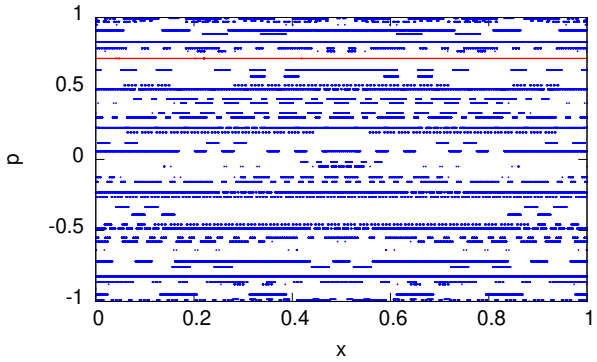

Figure 11: Invariant set of a billiard in a symmetric triangle with $\alpha = \beta = \pi(\sqrt{5}-1)/4$, which is obtained by lifting the line $p = p_0 = 0.7113433\ldots$ (red) to the phase space, see figure 10.

in a systematic way. Since the slow relaxation process is related with a localisation phenomenon for the momentum, see figure 2, it is promising to concentrate on this variable. However, as already pointed out in [17], the momentum itself does not possess a simple kind of evolution law. Following eq.(3) the change in momentum from its initial value can be reduced to integer variables, and the indices introduced in eq.(4) change little per time step. Hence, these quantities are useful for a statistical characterisation of the momentum dynamics, and the momentum index m_t completely determines the change of the momentum in symmetric triangles. Thus, unlike p itself, m_t can be easily employed to identify any localisation properties in phase space. A simple time series of m_t already shows that some logarithmic proliferation takes place for the billiard dynamics in symmetric irrational triangles. To obtain a feature which does not depend on the initial condition of a peculiar orbit we consider here the variance of the quantity m_t at fixed time, when we take a uniform average over initial conditions, $\langle (m_t)^2 \rangle_{Leb.}$. The variance quantifies the spread of momenta in phase space for typical initial conditions. The first moment vanishes due to symmetry and hence does not have to be taken into account when computing the variance.

The results in figure 12 clearly show a logarithmic time dependence of the variance and hence a slow proliferation of momenta in symmetric irrational triangles. A similar analysis can be performed for weakly asymmetric triangles to study the impact of symmetry breaking. While in the asymmetric case the momentum index alone does not determine the value of the momentum, one can still analyse this quantity, as it still encodes important features of the observed momentum spreading, in particular, in the weakly asymmetric case, see eq.(3). While initially the variance follows a logarithmic time dependence the phenomenon is transient and a transition towards a diffusive scaling is observed which becomes more pronounced when the symmetry breaking increases. Hence, asymmetric billiards are dominated by diffusive properties in momentum space while a logarithmic subdiffusive characteristic prevails in the symmetric case. These findings can be supplemented with results on distribution functions for the momentum index m_t. In the case of asymmetric triangles we obtain for large times a normal distribution, in line with the diffusive scaling of the

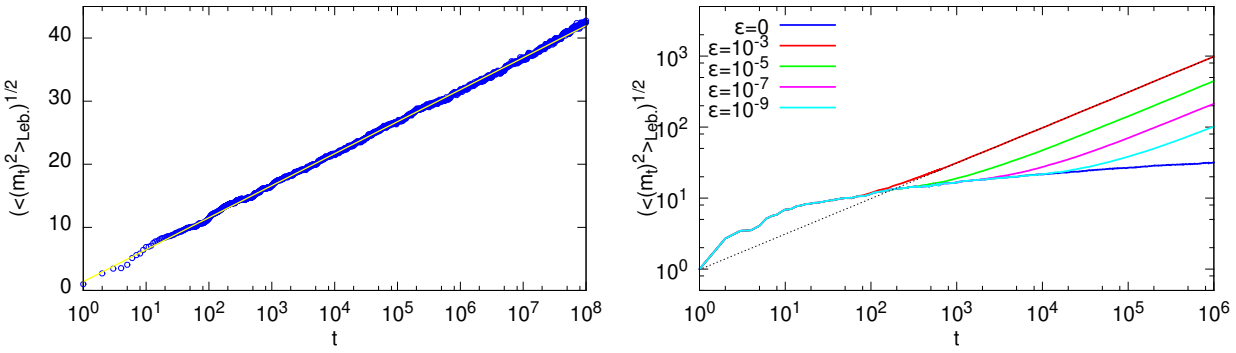

Figure 12: Standard deviation of the momentum index m_t, see eq.(4), as a function of time computed from an ensemble of initial conditions on a regular $p \times x = 500 \times 100$ grid in phase space. Left: standard deviation for a symmetric triangle $\alpha = \beta = \pi(\sqrt{5}-1)/4$ on a semi logarithmic scale. The straight line represents a least square fit $f(t) = a\log_{10}(t) + b$ with $a = 5.0709$ and $b = 1.3982$. Right: standard deviation on a double logarithmic scale for the symmetric ($\varepsilon = 0$) and weakly asymmetric triangles ($\varepsilon > 0$) with $\beta = \alpha - \varepsilon$. The dotted line represents a least square fit dt^c with $c = 0.4998$ and $d = 0.9836$.

variance and with claims in the literature, see e.g. [15]. In the symmetric case a different limit distribution is observed, see also [17] for similar results in related contexts. Since the variance increases in time, i.e., the distribution of m_t broadens in a logarithmic way, it is sensible to rescale the distribution by the standard deviation. Then the limit distribution seems to be close to an exponential distribution, see figure 13.

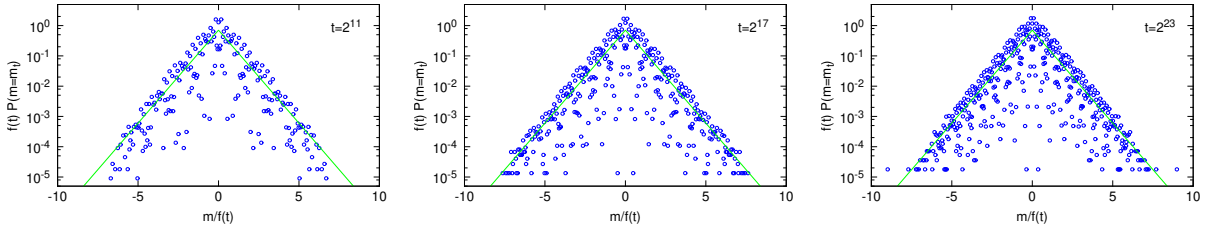

Figure 13: Distribution functions of the momentum index m_t for different values of time t, for a symmetric triangle with $\alpha = \beta = \pi(\sqrt{5}-1)/4$ (see figure 12). Ensemble averages have been computed for initial conditions on a regular $p \times x = 2000 \times 1000$ grid in phase space. Data have been shown on a normalised scale using a least square fit of the standard deviation $f(t) = a\log_{10}(t) + b$ with $a = 4.884$ and $b = 1.8965$. The line shows a standardised exponential distribution with variance one.

6. Conclusion

We have proven, for the very first time, the existence of one-dimensional induced maps, which govern the two-dimensional billiard dynamics in general symmetric triangles on suitable invariant sets. The construction of the invariant sets and the related interval exchange transformations make explicit use of the symmetry and are based on the prevalent recurrent dynamics which occurs in symmetric triangles. The dynamical structure we have uncovered constitutes the main mechanism for the anomalous dynamics of the momentum in symmetric triangular billiards since the recurrent dynamics only allows for a finite number of admissible values. Our construction is quite general and we believe that it applies for a dense set of initial conditions in phase space, but formal proofs for this conjecture are still missing.

The existence of interval exchange transformations for the billiard dynamics in symmetric irrational triangles has some striking similarity to the description in rational triangles. Because of the symmetry of the underlying billiard, recurrent orbits occur as conjugate pairs resulting in a special type of induced map, known as a symmetric interval exchange transformation, where the permutation of intervals is a symmetric permutation [22]. The discontinuities of the induced map are caused by singular orbits, while heteroclinic orbits are at the core of the construction of a well-defined induced map. All these elements also show up in the discussion of billiard dynamics in rational triangles.

The invariant sets in phase space on which the induced map acts provide a skeleton for the two-dimensional billiard dynamics. At a qualitative level the dynamics of the billiard may be considered as a meandering between these invariant sets and thus determines the characteristics of the dynamics on long but finite time scales. The resulting subdiffusive behaviour of the momentum which is responsible for the slow filling of the phase space is then caused by the tiny bottlenecks of the induced maps related with extremely high recurrence time. It could well be that the same mechanism is the reason for the observed scaling behaviour of the momentum index and the resulting exponential distribution. While we are currently lacking a formal proof, induced maps with high recurrence time may serve as a starting point to build up an analytic approach. Nevertheless, our considerations provide a convincing mechanism for the occurrence of subdiffusive behaviour which is intimately related to the symmetry of the triangle, and which does not occur in generic irrational billiards, where diffusive propagation of momentum and related normal distributions along the lines of the law of large numbers seems to prevail.

Our considerations may not be limited to the symmetric case, as other symmetries of the triangle could have similar impact. For instance, right angled and symmetric triangles are closely related by unfolding. While the relation between these billiards is not completely straightforward one can expect that some of the features visible for the symmetric case may pop up in the right angled case as well. Our analysis so far has focused on topological properties of symmetric irrational billiards. As such, these considerations have limited implications for the rigorous study of ergodic properties, if any. In fact, the ergodicity of a particular irrational triangular billiard is still a mystery from the rigorous perspective, apart from the very few explicit cases which are available in [12]. Nevertheless, our new approach to construct induced maps for symmetric triangular billiards may open up a new pathway to study billiard dynamics in irrational triangles employing the tools which have been already successfully applied in the rational case.

Postscriptum: After the manuscript was accepted the authors have been made aware of [28] (and references therein) which contains a rigorous underpinning of recurrence in a very broad class of polygonal billiards. This reference provides an alternative mathematical framework for some of the findings contained in the current manuscript.

References

[1] E. Gutkin, Billiards in polygons: Survey of recent results, J. Stat. Phys. 83 (1996) 7.
[2] N. Chernov, R. Markarian, Chaotic Billiards, Mathematical Surveys and Monographs, vol. 127, American Mathematical Society, 2006.
[3] H. Schachner, G. Obermair, Quantum billiards in the shape of right triangles, Z. Phys. B 95 (1994) 113.
[4] S. Panda, S. Maulik, S. Chakraborty, S. Khastgir, From classical periodic orbits in integrable π-rational billiards to quantum energy spectrum, Eur. Phys. J. Plus 134 (2019) 308.
[5] C. Lozej, G. Casati, T. Prosen, Quantum chaos in triangular billiards, Phys. Rev. Res. 4 (2022) 013138.
[6] A. N. Zemlyakov, A. B. Katok, Topological transitivity of billiards in polygons, Math. Notes Acad. Sci. USSR 18 (1975) 760.
[7] H. Masur, S. Tabachnikov, Rational billiards and flat structures, in: B. Hasselblatt, A. Katok (Eds.), Handbook of Dynamical Systems, Vol 1A, North Holland, Amsterdam, 2002, p. 1015.
[8] M. Viana, Ergodic theory of interval exchange maps, Rev. Mat. Comp. 19 (2006) 7.
[9] G. Rauzy, Echanges d'intervalles et transformations induites, Acta Arith. 34 (1979) 315.
[10] A. Katok, Interval exchange transformatiomns and some special flows are not mixing, Isr. J. Math. 35 (1980) 301.
[11] S. Kerckhoff, H. Masur, J. Smillie, Ergodicity of billiard flows and quadratic differentials, Ann. Math. 115 (1986) 293.
[12] Y. B. Vorobets, Ergodicity of billiards in polygons: explicit examples, Russ. Math. Surv. 51 (1996) 756.
[13] R. Artuso, G. Casati, I. Guarneri, Numerical study on ergodic properties of triagular billiards, Phys. Rev. E 55 (1997) 6384.
[14] G. Casati, T. Prosen, Mixing property of triangular billiards, Phys. Rev. Lett. 83 (1999) 4729.
[15] G. Casati, T. Prosen, Triangle map: A model of quantum chaos, Phys. Rev. Lett. 85 (2000) 4261.
[16] M. Horvat, M. D. Esposti, S. Isola, L. Bunimovich, On ergodic and mixing properties of the triangle map, Physica D 238 (2009) 395.
[17] J. Wang, G. Casati, T. Prosen, Nonergodicity and localization of invariant measure for two colliding masses, Phys. Rev. E 89 (2014) 042918.
[18] L. Kaplan, E. Heller, Weak quantum ergodicity, Physica D 121 (1998) 1.
[19] K. Zahradova, J. Slipantschuk, O. F. Bandtlow, W. Just, Impact of symmetry on ergodic properties of triangular billiards, Phys. Rev. E 105 (2022) L012201.
[20] G. Galperin, Non-periodic and not everywhere dense billiard trajectories in convex polygons and polyhedrons, Comm. Math. Phys. 91 (1983) 187.
[21] G. Tokarsky, Galperin's triangle example, Comm. Math. Phys. 335 (2015) 1211.
[22] S. Ferenczi, L. Zamboni, Structure of k-interval exchange transformations: Induction, trajectories, and distance theorems, J. Analy. Math. 112 (2010) 289.
[23] F. Beukers, J.-P. Bézivin, P. Robba, An alternative proof of the lindemann-weierstrass theorem, Amer. Math. Monthly 3 (1990) 193.
[24] J. Smillie, C. Ulcigrai, Beyond sturmian sequences: coding linear trajectories in the regular octagon, Proc. London Math. Soc. 102 (2010) 291.
[25] D. Davis, Cutting sequences, regular polygons, and the veech group, Geom. Dedi. 162 (2012) 231.
[26] Y. Shen, J. Yang, Hearing the shape of right triangular billiard tables, Discr. Cont. Dyn. Sys. 41 (2021) 5537.
[27] M. Duchin, V. Erlandsson, You can hear the shape of a billiard table: Symbolic dynamics and the rigidity for flat surfaces, Comment. Math. Helv. 96 (2021) 421.
[28] S. Troubetzkoy, Recurrence and periodic billiard orbits in polygons Regular and Chaotic Dynamics, 9 (2004) 1.